

AD-A272 604



2

**NAVAL POSTGRADUATE SCHOOL
Monterey, California**



S DTIC
ELECTE
NOV 16 1993
A

THESIS

**NUMERICAL MODELING OF A
PROPAGATING CRACK**

by

Clifford Christy

June 1993

Thesis Advisor:

Dr. Young W. Kwon

Approved for public release; distribution is unlimited.

93-27957



03

12 126

Unclassified

Security Classification of this page

REPORT DOCUMENTATION PAGE

| | | | | | |
|--|-------|-----------------------------|--|------------|----------------------------|
| 1a Report Security Classification: Unclassified | | | 1b Restrictive Markings | | |
| 2a Security Classification Authority | | | 3 Distribution/Availability of Report | | |
| 2b Declassification/Downgrading Schedule | | | Approved for public release; distribution is unlimited. | | |
| 4 Performing Organization Report Number(s) | | | 5 Monitoring Organization Report Number(s) | | |
| 6a Name of Performing Organization Naval Postgraduate School | | 6b Office Symbol 34 | 7a Name of Monitoring Organization Naval Postgraduate School | | |
| 6c Address (city, state, and ZIP code) Monterey CA 93943-5000 | | | 7b Address (city, state, and ZIP code) Monterey CA 93943-5000 | | |
| 8a Name of Funding/Sponsoring Organization | | 6b Office Symbol | 9 Procurement Instrument Identification Number | | |
| Address (city, state, and ZIP code) | | | 10 Source of Funding Numbers | | |
| | | | Program Element No | Project No | Task No |
| | | | Work Unit Accession No | | |
| 11 Title (include security classification) *NUMERICAL MODELING OF A PROPAGATING CRACK (UNCLASS) | | | | | |
| 12 Personal Author(s) *Clifford T. Christy | | | | | |
| 13a Type of Report Master's Thesis | | 13b Time Covered From To | 14 Date of Report (year, month, day) June 1993 | | 15 Page Count 58 |
| 16 Supplementary Notation The views expressed in this thesis are those of the author and do not reflect the official policy or position of the Department of Defense or the U.S. Government. | | | | | |
| 17 Cosati Codes | | | 18 Subject Terms (continue on reverse if necessary and identify by block number) | | |
| Field | Group | Subgroup | Crack propagation Stationary element | | |
| | | | Moving node element Central difference method | | |
| 19 Abstract (continue on reverse if necessary and identify by block number) | | | | | |
| <p>In the numerical modeling of the crack propagation in dynamic fracture using stationary elements, a discrete and sudden release of node at the crack tip creates spurious oscillation in the kinetic and strain energy values. In order to reduce the oscillation, a moving node element was utilized. This element can model a continuous crack tip movement more closely. The moving node element is compatible with surrounding regular isoparametric elements and no remeshing is required during the crack propagation. In addition, two different central difference schemes were compared, and their results were almost the same.</p> | | | | | |
| 20 Distribution/Availability of Abstract _x_ unclassified/unlimited __ same as report __ DTIC users | | | 21 Abstract Security Classification Unclassified | | |
| 22a Name of Responsible Individual Y.W. Kwon | | | 22b Telephone (include Area Code) 408-656-3385 | | 22c Office Symbol ME/KW |

DD FORM 1473,84 MAR

83 APR edition may be used until exhausted

All other editions are obsolete

security classification of this page

Unclassified

Approved for public release; distribution is unlimited.

Numerical Modeling of a Propagating Crack

by

Clifford T. Christy

Lieutenant, United States Navy

B.S., Pennsylvania State University, 1985

Submitted in partial fulfillment
of the requirements for the degree of

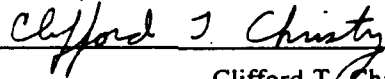
MASTER OF SCIENCE IN MECHANICAL ENGINEERING

from the

NAVAL POSTGRADUATE SCHOOL

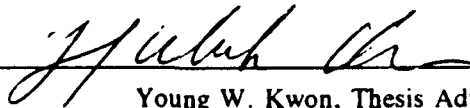
June 1993

Author:



Clifford T. Christy

Approved by:



Young W. Kwon, Thesis Advisor



Matthew D. Kelleher, Chairman

Department of Mechanical Engineering

ABSTRACT

In the numerical modeling of the crack propagation in dynamic fracture using stationary elements, a discrete and sudden release of node at the crack tip creates spurious oscillation in the kinetic and strain energy values. In order to reduce the oscillation, a moving node element was utilized. This element can model a continuous crack tip movement more closely. The moving node element is compatible with surrounding regular isoparametric elements and no remeshing is required during the crack propagation. In addition, two different central difference schemes were compared, and their results were almost the same.

TABLE OF CONTENTS

| | |
|---|----|
| I. INTRODUCTION | 1 |
| II. MATHEMATICAL DERIVATION | 7 |
| A. GOVERNING EQUATION | 7 |
| B. BOUNDARY CONDITIONS | 9 |
| C. MASS MATRIX | 12 |
| D. DAMPING MATRIX | 16 |
| E. STIFFNESS MATRIX | 16 |
| F. BODY FORCE VECTOR | 18 |
| G. LOAD VECTOR | 19 |
| H. TRANSIENT ANALYSIS | 21 |
| I. DYNAMIC FRACTURE ANALYSIS | 23 |
| III. RESULTS AND DISCUSSION | 26 |
| A. PROBLEM STATEMENT | 26 |
| B. VERIFICATION EXAMPLES | 27 |
| C. NUMERICAL TIME INTEGRATION | 29 |
| D. STUDY ON MASS AND STIFFNESS MATRICES | 32 |
| E. COMPARISONS OF ENERGY TERMS | 33 |
| IV. CONCLUSIONS AND RECOMMENDATIONS | 45 |

LIST OF REFERENCES 47

INITIAL DISTRIBUTION LIST 49

DTIC QUALITY INSPECTED 6

| | |
|--------------------|-------------------------------------|
| Accession For | |
| NTIS CRA&I | <input checked="" type="checkbox"/> |
| DTIC TAB | <input type="checkbox"/> |
| Unannounced | <input type="checkbox"/> |
| Justification | |
| By | |
| Distribution | |
| Availability Codes | |
| Dist | Avail and/or Special |
| A-1 | |

LIST OF FIGURES

| | |
|--|----|
| Figure 1. (a) Modeling of a propagating crack using a stationary node element. (b) An eight noded regular element. | 5 |
| Figure 2. (a) Modeling of a crack propagating using a moving node element. (b) An eight noded moving node element. | 6 |
| Figure 3. Fraction of total force on the element . . . | 20 |
| Figure 4. Displacement of end of beam | 28 |
| Figure 5. Relationship of beta to element length . . . | 32 |
| Figure 6. Effect of varying beta on strain energy for nstep1 = 50: (a) beta = 1/20, (b) beta = 1/10, (c) beta = 1/5. | 37 |
| Figure 7. Effect when node five is to close to corner node | 38 |
| Figure 8. Finite element mesh for Broberg's problem . . | 39 |
| Figure 9. Crack Opening Displacement for (a) stationary element and (b) moving node element | 40 |
| Figure 10. Crack opening displacement at x = 0 | 41 |
| Figure 11. Work vs Crack Length (a) stationary element, (b) moving node element (beta=1/5) | 42 |
| Figure 12. Strain energy vs Crack Length for (a) stationary element (b) moving node element (beta=1/5) | 43 |

Figure 13. Kinetic energy vs Crack Length for (a)
stationary element (b) moving node element
(beta=1/5) 44

ACKNOWLEDGEMENT

My deep appreciation is extended to Dr. Young W. Kwon for his support, guidance and encouragement throughout the course of this study.

I. INTRODUCTION

Inherent flaws in engineering materials can lead to a catastrophic failure due to unstable crack propagation. By eliminating the conditions and/or manufacturing defects (i.e., overloading, fabrication) which can lead to crack initiation, catastrophic failure can be prevented. In many structural components absolute prevention can not always be guaranteed. For such structures, catastrophic failure can be minimized by a crack arrest system. To ensure the proper incorporation of a crack arrest system, the effects of a propagating crack must be understood. These effects can be understood through the study of dynamic fracture mechanics.

Dynamic fracture mechanics can be applied to any problem involving a body containing a crack in which inertia forces play an important role. In practice two kinds of dynamic fracture problems have received the most attention [Ref. 1]. These are:

1. bodies with stationary cracks that are subjected to a rapidly varying load, and
2. bodies under fixed or slow varying loading that contain rapidly moving cracks.

Dynamic crack propagation can be divided into two categories: crack initiation and crack propagation. A third category sometimes used is crack arrest. There are different opinions concerning crack arrest. Kanninen [Ref. 2] asserted that crack arrest is not a separate category of dynamic crack propagation, but is the termination phase of crack propagation.

Dynamic fracture mechanics problems have focused mainly on bodies that contain a rapidly moving crack. As such, several numerical dynamic fracture analyses for the opening mode crack propagation have been studied. Kobayashi, et al. [Ref. 3] analyzed two fracturing Homalite-100 plates by dynamic finite element and dynamic photoelastic analyses. These analyses used the process of discrete crack-tip advances. The restraining nodal force was suddenly released when the crack-tip reached the next adjacent node. As indicated by Malluck and King [Ref. 4], the above procedure has inherent problems: the sudden release of a node can induce unwanted high-frequency of motions; and the crack tip location within the nodal spacing can not be determined. To reduce this problem Malluck and King incorporated a mechanism for energy release in their finite element analysis. The nodal reaction of the crack tip was gradually reduced as the crack tip propagated (in the continuum view) from one node to the next node.

Kobayashi, et al. [Ref. 5] were aware of the considerable oscillations in the calculated dynamic energy release rate.

They believed the oscillation was due to the sudden release of the crack tip (finite element nodes). To reduce these effects a nodal force release mechanism was incorporated to depict a more gradual transit of the crack tip between adjacent nodes. However, the assumed nodal release force is a somehow arbitrary choice.

As indicated in [Ref. 6], computational procedures for crack propagation problems can be grouped into two types: stationary mesh procedure and moving mesh procedure. The above analyses may be categorized as a stationary mesh procedure. To predict the continuing propagation of a crack in a discrete model closely, moving mesh procedures were introduced. Nishioka and Atluri [Ref. 7] analyzed the propagating crack using a moving singular element in which the geometry of the element was altered as the crack propagated; thereby, requiring remeshing of the elements after an elapse period of time. If the element is distorted severely the accuracy may be degraded as indicated in [Ref. 8]; therefore, it was critical that remeshing occurred at the appropriate time. Kwon and Akin [Ref. 9] developed a procedure for modeling the crack propagation problem using a node moving along the edge of the element. In this procedure the element is not distorted; therefore, remeshing is not required. A modification of the latter procedure was incorporated into this study.

The main objective of this study is to examine different numerical modeling techniques for studying dynamic crack

propagation. The main emphasis is placed on reducing the spurious oscillation in the calculated energy terms which resulted from the stationary node procedure, Figure 1a. An eight noded regular element (Figure 1b) was used in the procedure. To reduce the spurious oscillation a moving node procedure (Figure 2a) using a moving node (Figure 2b) was incorporated into the finite element model.

The study focused on the analysis of a rapidly propagating crack of opening mode in a linearly elastic isotropic body. Inertia was formulated into a diagonal mass matrix and the numerical time integration was accomplished using the two different central difference method. Crack propagation was simulated by the sequential release (at prescribe time intervals) of the nodes along the edge of the finite element model. Both stationary and moving node techniques were used to model the crack tip movement. Crack tip stress singularity was not represented in the model. From these method, crack opening displacement, work, strain energy, and kinetic energy were calculated and a comparative analysis was conducted from the results.

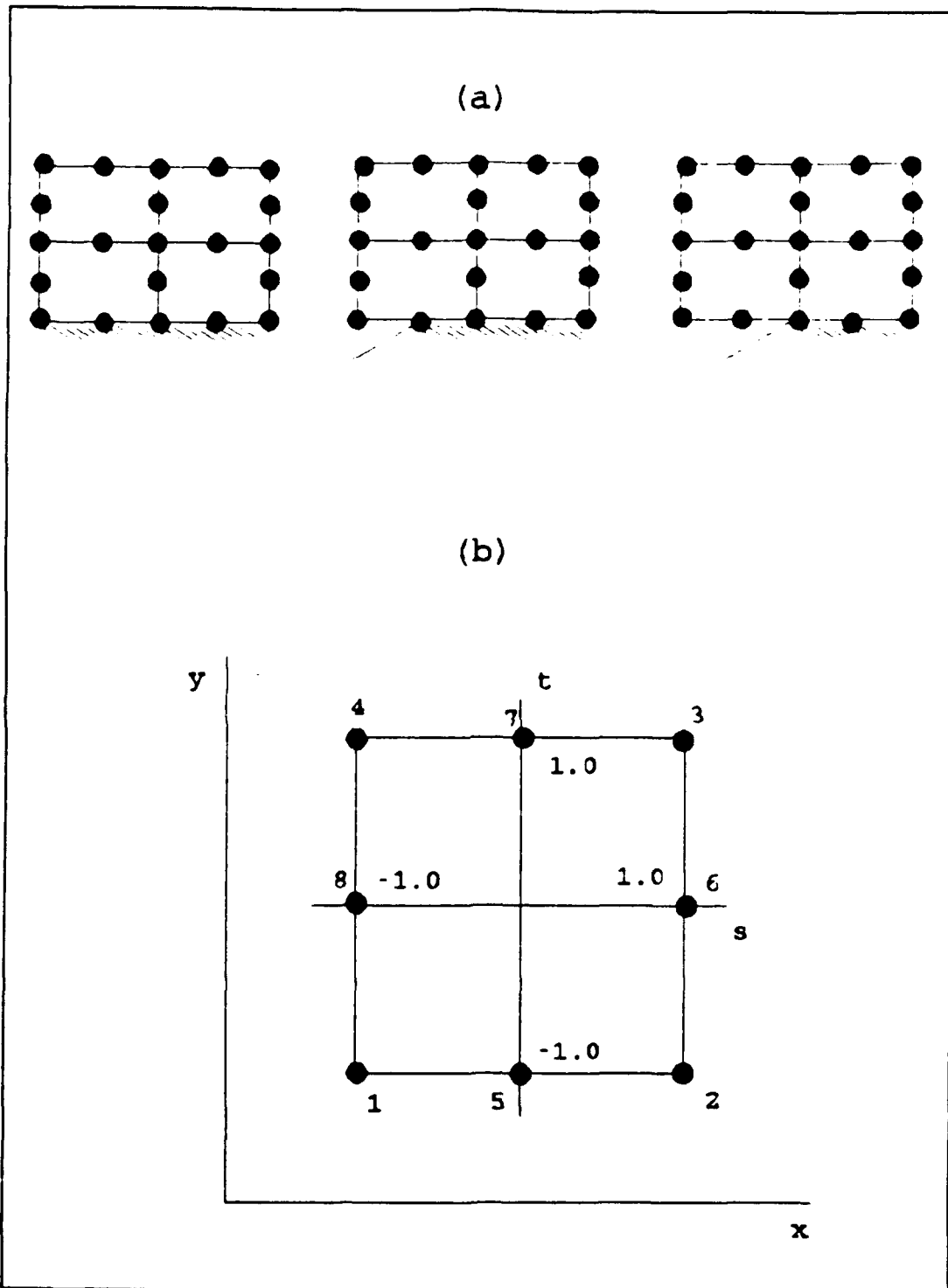


Figure 1. (a) Modeling of a propagating crack using a stationary node element. (b) An eight noded regular element.

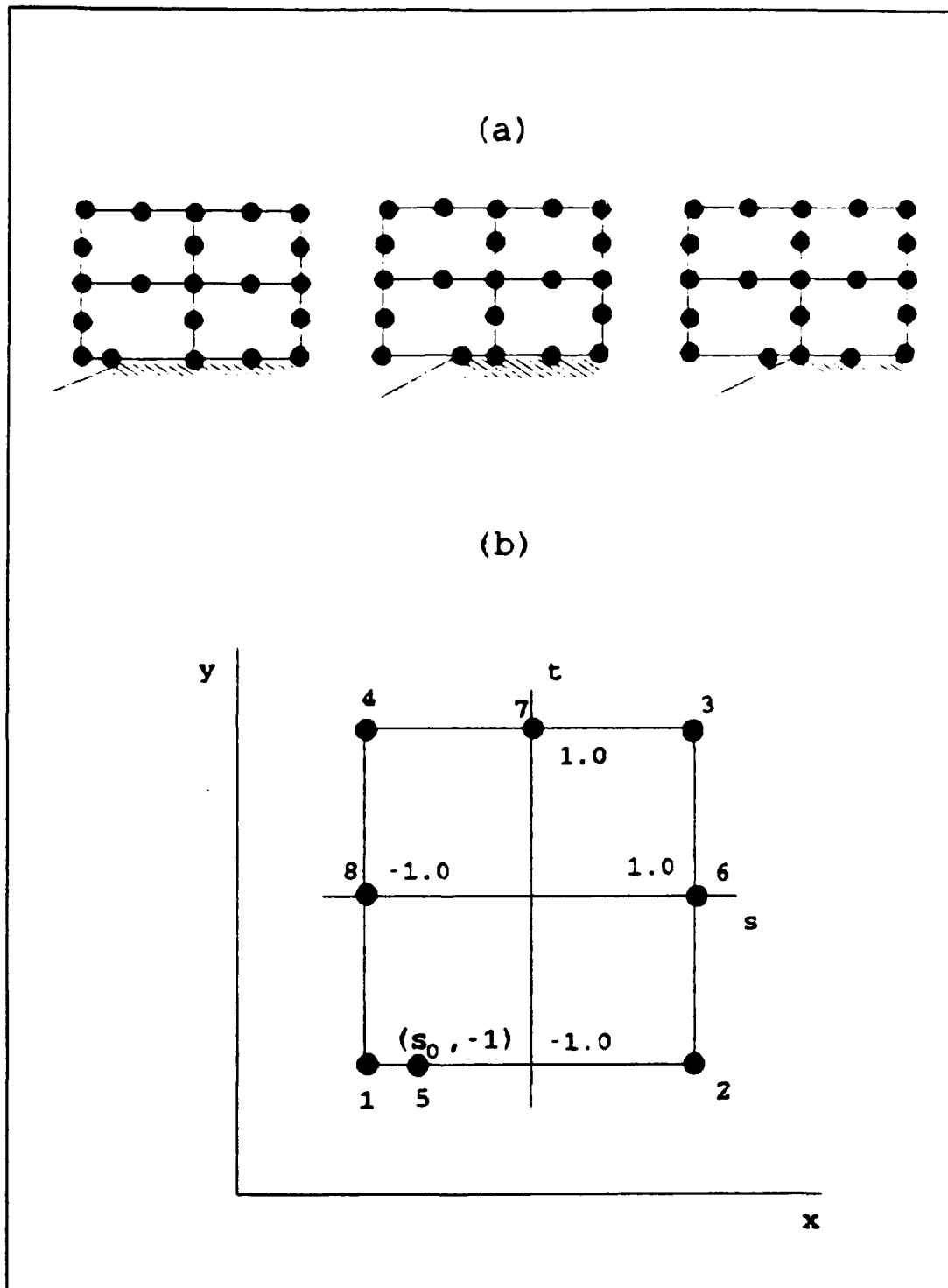


Figure 2. (a) Modeling of a crack propagating using a moving node element. (b) An eight noded moving node element.

II. MATHEMATICAL DERIVATION

A. GOVERNING EQUATION

In an elastodynamic problem of a continuous isotropic body, certain governing equations must be satisfied at all interior points of the body. For two-dimensional problems, the equations of motion are:

$$\begin{aligned}\frac{\partial \sigma_x}{\partial x} + \frac{\partial \tau_{xy}}{\partial y} - \mu \frac{\partial u}{\partial t} + F_x - \rho \frac{\partial^2 u}{\partial t^2} &= 0 \\ \frac{\partial \tau_{xy}}{\partial x} + \frac{\partial \sigma_y}{\partial y} - \mu \frac{\partial v}{\partial t} + F_y - \rho \frac{\partial^2 v}{\partial t^2} &= 0\end{aligned}\tag{1}$$

where σ_x , σ_y , and τ_{xy} are the normal stresses in the x and y direction and the shear stress, respectively. F_x and F_y are the body forces in the x and y direction, respectively. ρ is the density of the material. μ is the damping coefficient for the viscous damping. u and v are the displacements in the x and y direction, respectively. And t denotes the time.

The constitutive equation (stress-strain relations) is

$$\{\sigma\} = [D] \{\epsilon\}\tag{2}$$

where $\{\sigma\}$ represents the stress vector and $\{\epsilon\}$ the strain vector, as shown below:

$$\begin{aligned}\{\sigma\} &= [\sigma_x \ \sigma_y \ \tau_{xy}]^T \\ \{\epsilon\} &= [\epsilon_x \ \epsilon_y \ \gamma_{xy}]^T\end{aligned}\tag{3}$$

and $[D]$ is a symmetric 3×3 material property matrix. For an isotropic material, $[D]$ is

$$[D] = \frac{E}{(1-\nu^2)} \begin{bmatrix} 1 & \nu & 0 \\ \nu & 1 & 0 \\ 0 & 0 & \frac{1-\nu}{2} \end{bmatrix}\tag{4}$$

for the plane stress condition and

$$[D] = \frac{E(1-\nu)}{(1+\nu)(1-2\nu)} \begin{bmatrix} 1 & \frac{\nu}{1-\nu} & 0 \\ \frac{\nu}{1-\nu} & 1 & 0 \\ 0 & 0 & \frac{1-2\nu}{2(1-\nu)} \end{bmatrix}\tag{5}$$

for the plane strain condition.

The kinematic equation (strain-displacement relation) is

$$\begin{Bmatrix} \epsilon_x \\ \epsilon_y \\ \gamma_{xy} \end{Bmatrix} = \begin{Bmatrix} \frac{\partial u}{\partial x} \\ \frac{\partial v}{\partial y} \\ \frac{\partial u}{\partial y} + \frac{\partial v}{\partial x} \end{Bmatrix}\tag{6}$$

B. BOUNDARY CONDITIONS

In addition to satisfying the governing equations, the prescribed conditions on stress and/or displacement must be satisfied on the boundary surface of the body. These conditions are classified as below. The essential boundary conditions are

$$\begin{aligned}u &= \bar{u} \\v &= \bar{v}\end{aligned}\tag{7}$$

and the natural boundary conditions are

$$\begin{aligned}\phi_x &= \sigma_x n_x + \tau_{xy} n_y \\ \phi_y &= \tau_{xy} n_x + \sigma_y n_y\end{aligned}\tag{8}$$

where ϕ_x and ϕ_y are the traction in the x and y direction, respectively. And n_x and n_y are the components of the outward directed unit normal vector on the boundary surface in the x and y direction, respectively. Boundary value problems, in general, consist of a combination of the two types described above.

To transform the differential equations to matrix equations, apply the Galerkin method of weighted residual to the equations of motion (1):

$$I_1 = \int_{\Omega} \left(\frac{\partial \sigma_x}{\partial x} + \frac{\partial \tau_{xy}}{\partial y} - \mu \frac{\partial u}{\partial t} + F_x - \rho \frac{\partial^2 u}{\partial t^2} \right) \omega_1 d\Omega = 0 \quad (9)$$

$$I_2 = \int_{\Omega} \left(\frac{\partial \tau_{xy}}{\partial x} + \frac{\partial \sigma_y}{\partial y} - \mu \frac{\partial v}{\partial t} + F_y - \rho \frac{\partial^2 v}{\partial t^2} \right) \omega_2 d\Omega = 0$$

where ω_1 and ω_2 are test (weighing) functions and Ω is the domain of the given problem. Because Galerkin's method yields a non-symmetric matrix equation, apply the weak formulation to equation (9) to get a symmetric matrix. The results yield a symmetric equation because the governing equation is self-adjoint. Integrating by parts the stress terms of equation (9) yields:

$$I_1 = - \int_{\Omega} \left(\sigma_x \frac{\partial \omega_1}{\partial x} + \tau_{xy} \frac{\partial \omega_1}{\partial y} + \mu \frac{\partial u}{\partial t} \omega_1 - F_x \omega_1 + \rho \frac{\partial^2 u}{\partial t^2} \omega_1 \right) d\Omega + \int_{\Gamma} (\sigma_x n_x \omega_1 + \tau_{xy} n_y \omega_1) d\Gamma = 0 \quad (10)$$

$$I_2 = - \int_{\Omega} \left(\tau_{xy} \frac{\partial \omega_2}{\partial x} + \sigma_y \frac{\partial \omega_2}{\partial y} + \mu \frac{\partial v}{\partial t} \omega_2 - F_y \omega_2 + \rho \frac{\partial^2 v}{\partial t^2} \omega_2 \right) d\Omega + \int_{\Gamma} (\tau_{xy} n_x \omega_2 + \sigma_y n_y \omega_2) d\Gamma = 0$$

where Γ is the boundary surface of the domain Ω . Rewriting equation (10) into matrix form:

$$\int_{\Omega} \left(\begin{bmatrix} \frac{\partial \omega_1}{\partial x} & 0 & \frac{\partial \omega_1}{\partial y} \\ 0 & \frac{\partial \omega_2}{\partial y} & \frac{\partial \omega_2}{\partial x} \end{bmatrix} \begin{Bmatrix} \sigma_x \\ \sigma_y \\ \tau_{xy} \end{Bmatrix} + \rho \begin{bmatrix} \omega_1 & 0 \\ 0 & \omega_2 \end{bmatrix} \begin{Bmatrix} \frac{\partial^2 u}{\partial t^2} \\ \frac{\partial^2 v}{\partial t^2} \end{Bmatrix} + \mu \begin{bmatrix} \omega_1 & 0 \\ 0 & \omega_2 \end{bmatrix} \begin{Bmatrix} \frac{\partial u}{\partial t} \\ \frac{\partial v}{\partial t} \end{Bmatrix} \right) d\Omega = \quad (11)$$

$$\int_{\Gamma} \begin{Bmatrix} \phi_x \omega_1 \\ \phi_y \omega_2 \end{Bmatrix} d\Gamma + \int_{\Omega} \begin{bmatrix} \omega_1 & 0 \\ 0 & \omega_2 \end{bmatrix} \begin{Bmatrix} F_x \\ F_y \end{Bmatrix} d\Omega$$

where the first term becomes the stiffness matrix, the second term becomes mass matrix, the third term becomes the damping matrix, the fourth term becomes the load vector, and the fifth term becomes the body force vector. Substituting the constitutive equation (2) into (11) gives

$$\int_{\Omega} \left(\begin{bmatrix} \frac{\partial \omega_1}{\partial x} & 0 & \frac{\partial \omega_1}{\partial y} \\ 0 & \frac{\partial \omega_2}{\partial y} & \frac{\partial \omega_2}{\partial x} \end{bmatrix} [D] \begin{Bmatrix} \epsilon_x \\ \epsilon_y \\ \gamma_{xy} \end{Bmatrix} + \rho \begin{bmatrix} \omega_1 & 0 \\ 0 & \omega_2 \end{bmatrix} \begin{Bmatrix} \frac{\partial^2 u}{\partial t^2} \\ \frac{\partial^2 v}{\partial t^2} \end{Bmatrix} + \mu \begin{bmatrix} \omega_1 & 0 \\ 0 & \omega_2 \end{bmatrix} \begin{Bmatrix} \frac{\partial u}{\partial t} \\ \frac{\partial v}{\partial t} \end{Bmatrix} \right) d\Omega = \int_{\Gamma} \begin{Bmatrix} \phi_x \omega_1 \\ \phi_y \omega_2 \end{Bmatrix} d\Gamma + \int_{\Omega} \begin{bmatrix} \omega_1 & 0 \\ 0 & \omega_2 \end{bmatrix} \begin{Bmatrix} F_x \\ F_y \end{Bmatrix} d\Omega \quad (12)$$

Substituting the kinematic equation (6) into (12) gives

$$\int_{\Omega} \left(\begin{bmatrix} \frac{\partial \omega_1}{\partial x} & 0 & \frac{\partial \omega_1}{\partial y} \\ 0 & \frac{\partial \omega_2}{\partial y} & \frac{\partial \omega_2}{\partial x} \end{bmatrix} [D] \begin{Bmatrix} \frac{\partial u}{\partial x} \\ \frac{\partial v}{\partial y} \\ \frac{\partial u}{\partial y} + \frac{\partial v}{\partial x} \end{Bmatrix} + \rho \begin{bmatrix} \omega_1 & 0 \\ 0 & \omega_2 \end{bmatrix} \begin{Bmatrix} \frac{\partial^2 u}{\partial t^2} \\ \frac{\partial^2 v}{\partial t^2} \end{Bmatrix} + \mu \begin{bmatrix} \omega_1 & 0 \\ 0 & \omega_2 \end{bmatrix} \begin{Bmatrix} \frac{\partial u}{\partial t} \\ \frac{\partial v}{\partial t} \end{Bmatrix} \right) d\Omega = \int_{\Gamma} \begin{Bmatrix} \phi_x \omega_1 \\ \phi_y \omega_2 \end{Bmatrix} d\Gamma + \int_{\Omega} \begin{bmatrix} \omega_1 & 0 \\ 0 & \omega_2 \end{bmatrix} \begin{Bmatrix} F_x \\ F_y \end{Bmatrix} d\Omega \quad (13)$$

The matrices and the load vector are computed on the element level by discretization of the domain Ω and the boundary surface Γ :

$$\begin{aligned} \Omega &= \sum \Omega^e \\ \Gamma &= \sum \Gamma^e \end{aligned} \quad (14)$$

where Ω_e and Γ_e are the element domain and element boundary surface, respectively.

C. MASS MATRIX

The mass matrix comes from

$$\int_{\Omega} \rho \begin{bmatrix} \omega_1 & 0 \\ 0 & \omega_2 \end{bmatrix} \begin{Bmatrix} \frac{\partial^2 u}{\partial t^2} \\ \frac{\partial^2 v}{\partial t^2} \end{Bmatrix} d\Omega \quad (15)$$

In this study eight noded isoparametric elements were used for the finite element mesh. The finite element derivation for the eight noded element is shown in detail below. The element is shown in Figure 1b.

From variable interpolation,

$$\begin{aligned} u &= H_1 u_1 + H_2 u_2 + H_3 u_3 + H_4 u_4 + H_5 u_5 + H_6 u_6 + H_7 u_7 + H_8 u_8 \\ v &= H_1 v_1 + H_2 v_2 + H_3 v_3 + H_4 v_4 + H_5 v_5 + H_6 v_6 + H_7 v_7 + H_8 v_8 \end{aligned} \quad (16)$$

where u_i and v_i are the displacements in the x and y direction of the respective node and H_i are the shape functions at the respective node.

For the regular eight noded isoparametric element [Ref. 10] they are

$$\begin{aligned}
H_1 &= \frac{1}{4} (1-s) (1-t) (1+s+t) \\
H_2 &= \frac{1}{4} (1+s) (1-t) (s+t-1) \\
H_3 &= \frac{1}{4} (1+s) (1+t) (1+t) (s+t-1) \\
H_4 &= \frac{1}{4} (1-s) (1+t) (t-s-1) \\
H_5 &= \frac{1}{2} (1-t) (1-s^2) \\
H_6 &= \frac{1}{2} (1+s) (1-t^2) \\
H_7 &= \frac{1}{2} (1+t) (1-s^2) \\
H_8 &= \frac{1}{2} (1-s) (1-t^2)
\end{aligned} \tag{17}$$

and for the eight noded isoparametric moving node element [Ref. 9] they are

$$\begin{aligned}
H_1 &= \frac{1}{4} (1-s) (1-t) - \frac{1-s_0}{2} H_5 - \frac{1}{2} H_8 \\
H_2 &= \frac{1}{4} (1+s) (1-t) - \frac{1+s_0}{2} H_5 - \frac{1}{2} H_6 \\
H_3 &= \frac{1}{4} (1+s) (1+t) - \frac{1}{2} H_6 - \frac{1}{2} H_7 \\
H_4 &= \frac{1}{4} (1-s) (1+t) - \frac{1}{2} H_7 - \frac{1}{2} H_8 \\
H_5 &= \frac{1}{2(1-s_0^2)} (1-s^2) (1-t) \\
H_6 &= \frac{1}{2} (1+s) (1-t^2) \\
H_7 &= \frac{1}{2} (1+t) (1-s^2) \\
H_8 &= \frac{1}{2} (1-s) (1-t^2)
\end{aligned} \tag{18}$$

Since the shape functions are independent the time, the acceleration terms are

$$\begin{Bmatrix} \frac{\partial^2 u}{\partial t^2} \\ \frac{\partial^2 v}{\partial t^2} \end{Bmatrix} = \begin{bmatrix} H_1 & 0 & H_2 & 0 & H_3 & 0 & H_4 & 0 & H_5 & 0 & H_6 & 0 & H_7 & 0 & H_8 & 0 \\ 0 & H_1 & 0 & H_2 & 0 & H_3 & 0 & H_4 & 0 & H_5 & 0 & H_6 & 0 & H_7 & 0 & H_8 \end{bmatrix} \begin{Bmatrix} \ddot{u}_1 \\ \ddot{v}_1 \\ : \\ : \\ \ddot{u}_8 \\ \ddot{v}_8 \end{Bmatrix} \quad (19)$$

Applying Galerkin's method

$$\begin{bmatrix} \omega_1 & 0 \\ 0 & \omega_2 \end{bmatrix} = \begin{bmatrix} H_1 & 0 & H_2 & 0 & H_3 & 0 & H_4 & 0 & H_5 & 0 & H_6 & 0 & H_7 & 0 & H_8 & 0 \\ 0 & H_1 & 0 & H_2 & 0 & H_3 & 0 & H_4 & 0 & H_5 & 0 & H_6 & 0 & H_7 & 0 & H_8 \end{bmatrix}^T \quad (20)$$

Substituting equations (19) and (20) into (15) gives

$$\int_{\Omega} \rho \begin{bmatrix} H_1 & 0 \\ 0 & H_1 \\ H_2 & 0 \\ 0 & H_2 \\ : & : \\ : & : \\ H_8 & 0 \\ 0 & H_8 \end{bmatrix} \begin{bmatrix} H_1 & 0 & H_2 & 0 & \dots & H_8 & 0 \\ 0 & H_1 & 0 & H_2 & \dots & 0 & H_8 \end{bmatrix} d\Omega \begin{Bmatrix} \ddot{u}_1 \\ \ddot{v}_1 \\ : \\ : \\ \ddot{u}_8 \\ \ddot{v}_8 \end{Bmatrix} \quad (21)$$

Since the shape functions are expressed in the natural coordinates, it is necessary to carry out the integration in equation (21) in the natural coordinate, using the relationship

$$d\Omega = dx dy = \det [J] ds dt \quad (22)$$

where $[J]$ is the Jacobian matrix given as

$$[J] = \begin{bmatrix} \frac{\partial x}{\partial s} & \frac{\partial y}{\partial s} \\ \frac{\partial x}{\partial \tau} & \frac{\partial y}{\partial \tau} \end{bmatrix} \quad (23)$$

Substituting equation (22) into (21) yields

$$\int_{-1}^1 \int_{-1}^1 \rho \begin{bmatrix} H_1 H_1 & 0 & H_1 H_2 & 0 & \dots & H_1 H_8 & 0 \\ 0 & H_1 H_1 & 0 & H_1 H_2 & \dots & 0 & H_1 H_8 \\ H_2 H_1 & 0 & H_2 H_2 & 0 & \dots & H_2 H_8 & 0 \\ 0 & H_2 H_1 & 0 & H_2 H_2 & \dots & 0 & H_2 H_8 \\ H_3 H_1 & 0 & H_3 H_2 & 0 & \dots & H_3 H_8 & 0 \\ 0 & H_3 H_1 & 0 & H_3 H_2 & \dots & 0 & H_3 H_8 \\ : & : & : & : & \dots & : & : \\ : & : & : & : & \dots & : & : \\ H_8 H_1 & 0 & H_8 H_2 & 0 & \dots & H_8 H_8 & 0 \\ 0 & H_8 H_1 & 0 & H_8 H_2 & \dots & 0 & H_8 H_8 \end{bmatrix} \det [J] ds d\tau \begin{Bmatrix} u_1 \\ v_1 \\ u_2 \\ v_2 \\ : \\ : \\ u_4 \\ v_4 \\ : \\ : \\ u_8 \\ v_8 \end{Bmatrix} \quad (24)$$

Since the shape functions are an explicit function of s and τ , a numerical method is used to evaluate equation (24). The two-point Gaussian quadrature formula is used to carry out the integration. The result is a symmetric consistent mass matrix.

For this study the consistent mass matrix was diagonalized by following procedure [Ref. 11]:

- a. Calculate the diagonal coefficients of the consistent mass matrix.

- b. Determine the total mass of the element, m .
- c. Add the diagonal coefficients, m_{ii} , associated with translation only to obtain a number, e .
- d. Multiply the diagonal coefficients, m_{ii} , by m/e .
- e. Set all the off-diagonal terms to zeros.

D. DAMPING MATRIX

The damping matrix is given by

$$\int_{\Omega} \mu \begin{bmatrix} \omega_1 & 0 \\ 0 & \omega_2 \end{bmatrix} \begin{Bmatrix} \frac{\partial u}{\partial \tau} \\ \frac{\partial v}{\partial \tau} \end{Bmatrix} d\Omega \quad (25)$$

Since the shape functions are independent of time,

$$\begin{Bmatrix} \frac{\partial u}{\partial \tau} \\ \frac{\partial v}{\partial \tau} \end{Bmatrix} = \begin{bmatrix} H_1 & 0 & H_2 & 0 & H_3 & 0 & H_4 & 0 & H_5 & 0 & H_6 & 0 & H_7 & 0 & H_8 & 0 \\ 0 & H_1 & 0 & H_2 & 0 & H_3 & 0 & H_4 & 0 & H_5 & 0 & H_6 & 0 & H_7 & 0 & H_8 \end{bmatrix} \begin{Bmatrix} \dot{u}_1 \\ \dot{v}_1 \\ : \\ : \\ \dot{u}_8 \\ \dot{v}_8 \end{Bmatrix} \quad (26)$$

Substituting equations (20), (22) and (26) into (25) and applying the two-point Gaussian formula gives a symmetric consistent damping matrix.

E. STIFFNESS MATRIX

The stiffness matrix is given as

$$\int_{\Omega^e} \begin{bmatrix} \frac{\partial \omega_1}{\partial x} & 0 & \frac{\partial \omega_1}{\partial y} \\ 0 & \frac{\partial \omega_2}{\partial y} & \frac{\partial \omega_2}{\partial x} \end{bmatrix} [D] \begin{Bmatrix} \frac{\partial u}{\partial x} \\ \frac{\partial v}{\partial y} \\ \frac{\partial u}{\partial y} + \frac{\partial v}{\partial x} \end{Bmatrix} d\Omega \quad (27)$$

Rewriting the kinematic equation in terms of nodal displacements gives

$$\begin{Bmatrix} \frac{\partial u}{\partial x} \\ \frac{\partial v}{\partial y} \\ \frac{\partial u}{\partial y} + \frac{\partial v}{\partial x} \end{Bmatrix} = \begin{bmatrix} \frac{\partial}{\partial x} & 0 & \frac{\partial}{\partial y} \\ 0 & \frac{\partial}{\partial y} & \frac{\partial}{\partial x} \end{bmatrix} \begin{Bmatrix} u \\ v \end{Bmatrix} = \quad (28)$$

$$\begin{bmatrix} \frac{\partial H_1}{\partial x} & 0 & \frac{\partial H_2}{\partial x} & 0 & \dots & 0 & \frac{\partial H_7}{\partial x} & 0 & \frac{\partial H_8}{\partial x} \\ 0 & \frac{\partial H_1}{\partial y} & 0 & \frac{\partial H_2}{\partial y} & \dots & 0 & \frac{\partial H_7}{\partial y} & 0 & \frac{\partial H_8}{\partial y} \\ \frac{\partial H_1}{\partial y} & \frac{\partial H_1}{\partial x} & \frac{\partial H_2}{\partial y} & \frac{\partial H_2}{\partial x} & \dots & \frac{\partial H_7}{\partial y} & \frac{\partial H_7}{\partial x} & \frac{\partial H_8}{\partial y} & \frac{\partial H_8}{\partial x} \end{bmatrix} \begin{Bmatrix} u_1 \\ v_1 \\ : \\ : \\ u_8 \\ v_8 \end{Bmatrix}$$

where

$$\begin{aligned} \frac{\partial H_i}{\partial x} &= \Lambda_{11} \frac{\partial H_i}{\partial s} + \Lambda_{12} \frac{\partial H_i}{\partial t} \\ \frac{\partial H_i}{\partial y} &= \Lambda_{21} \frac{\partial H_i}{\partial s} + \Lambda_{22} \frac{\partial H_i}{\partial t} \end{aligned} \quad (29)$$

and Λ_{ij} are the components of the inverse of the Jacobian matrix. The matrix in equation (28) is called the [B] matrix

and the vector is called the displacement vector $\{d\}$. From Galerkin's method on the first matrix in equation (27) gives

$$\begin{bmatrix} \frac{\partial \omega_1}{\partial x} & 0 & \frac{\partial \omega_1}{\partial y} \\ 0 & \frac{\partial \omega_2}{\partial y} & \frac{\partial \omega_2}{\partial x} \end{bmatrix} = [B]^T \quad (30)$$

Substituting equations (29) and (30) into (28) gives

$$\int_{\Omega^e} [B]^T [D] [B] d\Omega \{d\} \quad (31)$$

The stiffness matrix is given as

$$[K^e] = \int_{\Omega^e} [B]^T [D] [B] d\Omega \quad (32)$$

Substituting equation (22) into (32) gives

$$[K^e] = \int_{-1}^1 \int_{-1}^1 [B]^T [D] [B] \det [J] ds dt \quad (33)$$

The two-point Gaussian quadrature formula is used to carry out the integration.

F. BODY FORCE VECTOR

The body force vector is given as

$$\int_{\Omega} \begin{bmatrix} \omega_1 & 0 \\ 0 & \omega_2 \end{bmatrix} \begin{Bmatrix} F_x \\ F_y \end{Bmatrix} d\Omega \quad (34)$$

Substituting equations (20) and (22) into (34) gives

$$\int_{-1}^1 \int_{-1}^1 \begin{bmatrix} H_1 & 0 & H_2 & 0 & \dots & H_7 & 0 & H_8 & 0 \\ 0 & H_1 & 0 & H_2 & \dots & 0 & H_7 & 0 & H_8 \end{bmatrix}^T \begin{Bmatrix} F_x \\ F_y \end{Bmatrix} \det [J] ds dt \quad (35)$$

The two-point Gaussian quadrature formula is used to carry out the integration.

G. LOAD VECTOR

The load vector is given by

$$\int_{\Gamma} \begin{Bmatrix} \phi_x \omega_1 \\ \phi_y \omega_2 \end{Bmatrix} d\Gamma \quad (36)$$

where Γ is the boundary surface of the domain Ω . If there is no traction

$$\int_{\Gamma} \begin{Bmatrix} \phi_x \omega_1 \\ \phi_y \omega_2 \end{Bmatrix} d\Gamma = 0 \quad (37)$$

If there is traction, substituting equation (20) into (36) gives

$$\{P\} = \int_{4-7-3} \begin{bmatrix} \overline{H_4} & 0 & \overline{H_7} & 0 & \overline{H_3} & 0 \\ 0 & \overline{H_4} & 0 & \overline{H_7} & 0 & \overline{H_3} \end{bmatrix}^T \begin{Bmatrix} \phi_x \\ \phi_y \end{Bmatrix} \frac{L}{2} (h) ds \quad (38)$$

where $\{P\}$ is the external load vector along edge 4-7-3 (Figure 3), h is the element thickness and overbars indicate the shape functions H_i are evaluated at $t=1$ (the natural coordinate). Integrating equation (38) yields

$$\{P\} = \begin{Bmatrix} \phi_x \\ \phi_y \end{Bmatrix} hL \begin{Bmatrix} \frac{1}{6} & \frac{2}{3} & \frac{1}{6} \end{Bmatrix} \quad (39)$$

Fraction of the total force is shown in Figure 3.

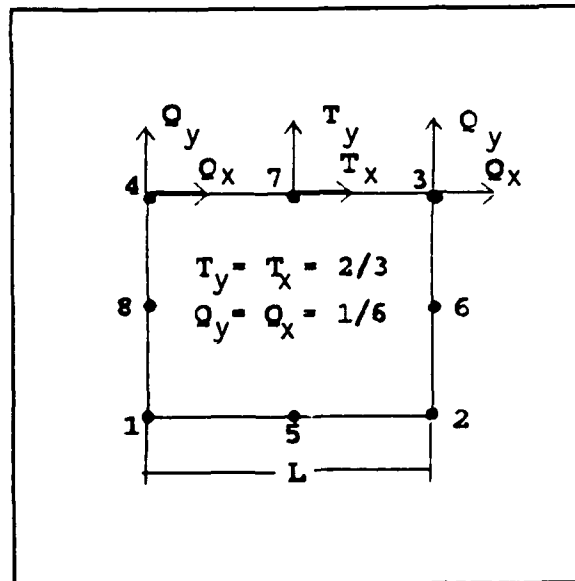


Figure 3. Fraction of total force on the element

From the procedural derivation above, the equation of motion is finally rewritten as

$$[M] \{\ddot{d}\} + [C] \{\dot{d}\} + [K] \{d\} = \{R\} \quad (40)$$

where $\{R\} = \{P\} + \{F\}$. This equation applies to any dynamic problem in which the finite element method is used.

H. TRANSIENT ANALYSIS

In dynamic problems the displacements, velocities, accelerations, strains, stresses, and loads are time dependent. Therefore, a time integration scheme is required. The equation of motion at time t is

$$[M] \{\ddot{d}\}^t + [C] \{\dot{d}\}^t + [K] \{d\}^t = \{R\}^t \quad (41)$$

This study examined two different forms of the central difference method:

The first method is as summarized below [Ref. 12];

A. Initial Calculations

1. Solve for $[M]$, $[C]$, and $[K]$
2. $\{\ddot{d}\}^t = [M]^{-1} [\{R\}^0 - [C] \{\dot{d}\}^0 - [K] \{d\}^0]$.
where $\{d\}^0$ and $\{\dot{d}\}^0$ are the initial conditions.
3. $\{d\}^{-\Delta t} = \{d\}^0 - (\Delta t) \{\dot{d}\}^0 + a_3 \{\ddot{d}\}^0$.
4. $[\tilde{M}] = a_0 [M] + a_1 [C]$.

B. For each time step

1. $\{\tilde{R}\} = \{R\}^t - ([K] - a_2[M])\{u\}^t - (a_0[M] - a_1[C])\{d\}^{t-\Delta t}$.
2. $\{d\}^{t+\Delta t} = [\tilde{M}]^{-1}\{\tilde{R}\}^t$.
3. $\{\ddot{d}\}^t = a_0[\{d\}^{t+\Delta t} - 2\{d\}^t + \{d\}^{t-\Delta t}]$.
4. $\{\dot{d}\}^t = a_1[\{d\}^{t+\Delta t} - \{d\}^{t-\Delta t}]$

where $a_0 = 1/\Delta t^2$; $a_1 = 1/2\Delta t$; $a_2 = 2a_0$; $a_3 = 1/a_2$

The second form "summed form" [Ref. 13] is as follows:

A. For each time step

1. $\{\ddot{d}\}^{\Delta t+1} = [M]^{-1}(R^{\Delta t+1} - [K]\{d\}^{\Delta t+1})$.
2. $\{\dot{d}\}^{\Delta t+3/2} = \{\dot{d}\}^{\Delta t+1/2} + \Delta t^{\Delta t+1}\{\ddot{d}\}^{\Delta t+1}$.
3. $\{d\}^{\Delta t+2} = \{d\}^{\Delta t+1} + \Delta t^{\Delta t+3/2}\{\dot{d}\}^{\Delta t+3/2}$.

The explicit central difference scheme is conditionally stable. The time step Δt must be controlled from the smallest period of the system. As indicated in [Ref. 14], a safe limiting value is given by

$$\Delta t = 0.45 L^n \left[\frac{\rho(1+\nu)(1-2\nu)}{E(1-\nu)} \right]^{1/2} \quad (42)$$

where L^n is the smallest distance between adjacent nodes of any element used and E and ν are the elastic modulus and poisson's ratio, respectively. This safe limiting value was used as a criteria to ensure stability.

I. DYNAMIC FRACTURE ANALYSIS

From elasticity the stresses near a crack tip for the opening mode are:

$$\begin{aligned}\sigma_x &= \frac{K}{\sqrt{2\pi r}} \cos \frac{\theta}{2} \left(1 - \sin \frac{\theta}{2} \sin \frac{3\theta}{2} \right) \\ \sigma_y &= \frac{K}{\sqrt{2\pi r}} \cos \frac{\theta}{2} \left(1 + \sin \frac{\theta}{2} \sin \frac{3\theta}{2} \right) \\ \tau_{xy} &= \frac{K}{\sqrt{2\pi r}} \left(\sin \frac{\theta}{2} \cos \frac{\theta}{2} \cos \frac{3\theta}{2} \right)\end{aligned}\tag{43}$$

where σ_x and σ_y are the tensile stresses in the x and y direction, respectively, τ_{xy} is the shear stress, r is the radial distance from the crack tip, θ is the angle from the crack plane, and K is the stress intensity factor. The stress intensity factor provides a convenient parameter of the stress distribution around a flaw. If K is equal to or exceeds a critical value (fracture toughness, K_c) the crack becomes unstable. K_c is a material property. [Ref. 15]

In the dynamic generalization of linear elastic fracture mechanics (LEFM), K_c has two parts. For the initiation of crack growth

$$K(a, \sigma, t) = K_d(\dot{\sigma})\tag{44}$$

where a represents the crack length, σ is the applied stress, t is time, and $\dot{\sigma}$ is the loading rate. Similarly, for a propagation crack

$$K(a, \sigma, t) = K_D(\dot{a}) \quad (45)$$

where \dot{a} denotes the crack speed. [Ref. 2]

An alternative criterion for determining the motion of a crack is,

$$G(a, \sigma, t) = R(\dot{a}) \quad (46)$$

where R is the energy dissipation rate required for crack growth and G is the dynamic energy release rate given by,

$$\begin{aligned} G &= \frac{1}{b} \left\{ \frac{dW}{da} - \frac{dU}{da} - \frac{dT}{da} \right\} \\ &= \frac{1}{b\dot{a}} \left\{ \frac{dW}{dt} - \frac{dU}{dt} - \frac{dT}{dt} \right\} \end{aligned} \quad (47)$$

where U is the strain energy, T is the kinetic energy, W is the work done on the structure by external loads, a is the crack length, and b is the plate thickness at the crack tip.

The dynamic energy release rate and the dynamic stress intensity factor are connected through Freund's formula,

$$K_D = \left\{ \frac{EG}{1-\nu^2} A(\dot{a}) \right\}^{\frac{1}{2}} \quad (48)$$

where G is the dynamic energy release rate, E is Young's modulus, ν is Poisson's ratio, and A is a function that is dependent on crack speed. A is given as

$$A = \frac{\left(\frac{\dot{a}}{C_2}\right)^2 \left(1 - \frac{\dot{a}^2}{C_1^2}\right)^{\frac{1}{2}}}{(1-\nu) \left[4 \left(1 - \frac{\dot{a}^2}{C_1^2}\right)^{\frac{1}{2}} \left(1 - \frac{\dot{a}^2}{C_2^2}\right)^{\frac{1}{2}} - \left(2 - \frac{\dot{a}^2}{C_2^2}\right)^2 \right]} \quad (49)$$

where C_1 and C_2 are the longitudinal and shear wave speeds.

[Ref. 2]

The wave speeds are given by [Ref. 16],

$$C_1 = \left[\frac{\lambda + 2\mu}{\rho} \right]^{\frac{1}{2}} \quad (50)$$

where λ and μ are Lamè's constants, and

$$C_2 = \left(\frac{\mu}{\rho} \right)^{\frac{1}{2}} \quad (51)$$

III. RESULTS AND DISCUSSION

A. PROBLEM STATEMENT

The main objective is how to best approximate the behavior of a continuous propagating crack using a discrete finite element model. The model was composed of a uniform mesh of eight noded isoparametric elements. In the first model the nodes were stationary. To approximate the movement of the crack, the nodal restraints were suddenly released at given time intervals (time required for the crack to travel a nodal spacing in the continuous movement). As will be shown, this resulted in spurious oscillation in the energy terms. To reduce the oscillation due to discrete jumps of the crack movement, as simulated by the model, a moving node element was employed in the second model.

Each of the analysis was based upon the plane-strain conditions of a centered cracked plate of homogeneous isotropic elastic material. The plate deformed under the action of an applied time-independent (constant) traction. The applied load was normal to the crack plane, mode I configuration. The mass matrix was diagonalized and the numerical time integration was accomplished by two different

forms of the central difference method. A comparative study was conducted of the two forms.

B. VERIFICATION EXAMPLES

The developed finite element analysis code was verified by analyzing a problem with a known solution. The problem considered is governed by the wave equation. A long uniform rod with one end fixed and the other end free was examined. The free end was subjected to an applied axial force which was released at time zero. Applying Newton's second law and for a constant area multiply by Young's modulus (AE) the equation of motion simplified to the wave equation

$$\frac{\partial^2 u}{\partial t^2} = c^2 \frac{\partial^2 u}{\partial x^2} \quad (51)$$

where $c^2 = E/\rho$ and u is the axial displacement of an element of the rod. By the method of separation of variables, the analytical solution is expressed as

$$u(x, t) = \frac{8FL}{\pi^2 AE} \sum_{n=0}^{\infty} \frac{(-1)^n}{(2n+1)^2} \sin \frac{(2n+1)\pi x}{2L} \cos \frac{(2n+1)\pi ct}{2L} \quad (52)$$

As shown in Figure 4, the numerical result was reasonably accurate. To verify the accuracy of the second model (moving node), it was compared to the stationary model when node five was at the center edge of the element. For this case the results should be and were the same.

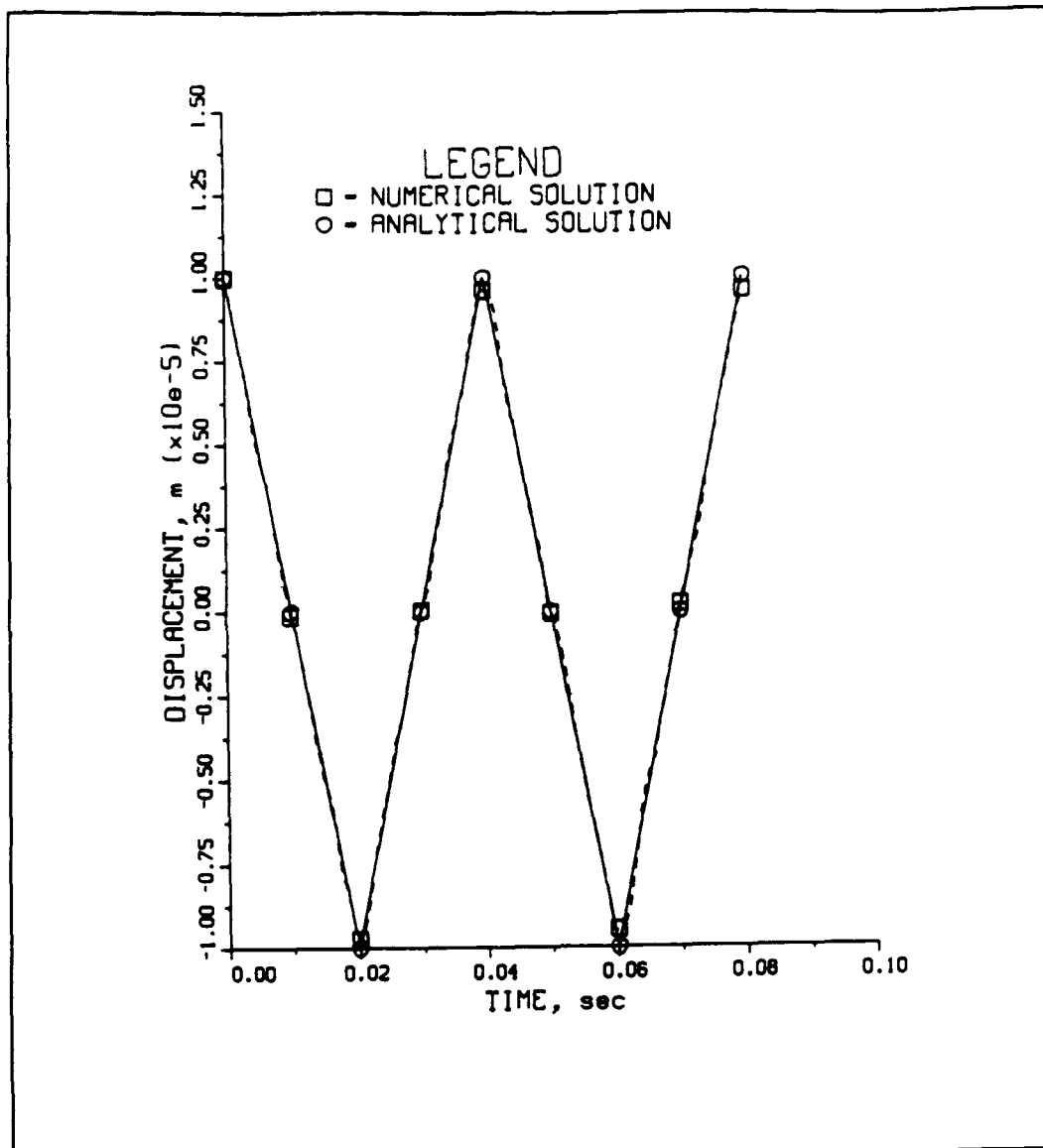


Figure 4. Displacement of end of beam

As another comparative check of the accuracy of the developed methods, the results of the crack opening displacement (COD) was compared against the analytical solution as derived by Broberg [Ref. 17]. To obtain the mathematical description of a two-dimensional crack, Broberg made the following assumption [Ref. 17]:

1. A two-dimensional crack can propagate in one plane only.
2. The material is homogeneous and isotropic with regard to fracturing characteristics and stress-strain relations.
3. The material obeys Hooke's law and is perfectly brittle.
4. The surface energy is zero.
5. The crack propagates with a maximum velocity from the start.

Broberg's analytical solution applies to an infinite medium with the above characteristics. These assumptions were incorporated into this study. The comparison between analytical and numerical solutions are shown later.

C. NUMERICAL TIME INTEGRATION

An explicit procedure based on the central difference method was incorporated into this study. The two forms of the method are as outlined in Chapter II. The latter is the "summed form" [Ref. 13]. From a computational consideration, the "summed form" has an advantage. For a damped structure, the "summed form" only requires the mass matrix be diagonalized to simplify the computation; whereas, the former

requires the diagonalization of the mass and damping matrix for simplification. To date no supporting argument or test cases exist which justifies the use of a diagonal damping matrix.

During the study it was noted that the first central difference method was very sensitive to computational round off errors. As the time increment decreased, the central difference did not converge while running the model in single precision. The model was ran at double precision (minimizing round off error) to achieve convergence. On the other hand, the "summed form" converged during single precision runs. Comparison of the convergent results revealed no difference between the two central difference techniques. The "summed form" simplifies the computation, and as a result, it saves time and money.

An important consideration when using the central difference method is the time step. Because the central difference method is conditionally stable, the time step must be less than the critical time step to ensure stability. The critical time step is defined as the time required for an acoustic wave to transverse the smallest element of the system [Ref. 11]. A time step less than the critical time step guarantees the stability of the solution. Stability meaning that the displacement does not grow without limit. As indicated in [Ref. 11], the practical limit on Δt is approximately 25% less than $2/\omega_{\max}$. As seen in this study,

decreasing the time step size considerably below the approximate formula for Δt_{cr} , equation (42), resulted in no change.

In the second analysis, the distance the moving node can travel is limited by β . β is the fractional distance of the element length. It represents the minimum distance the moving node should be from the corner node, Figure 5. Because convergence had occurred, decreasing Δt for a constant beta resulted in no change in the solutions. The minimum distance from the corner node, β , is dependent on Δt for relatively large time step size. As shown in Figure 6, decreasing β for a constant Δt introduced higher frequencies with similar magnitudes. If the moving node propagated within the minimum allowable distance, the system became unstable. Exceptionally high frequencies and amplitudes resulted, Figure 7.

As shown in the Table 1, further decreasing the time steps resulted in a constant β .

Table 1. Fractional minimum distance of the moving mid-node from the end node

| | | | | |
|------------------|-----|------|------|------|
| NSTEP | 10 | 25 | 50 | 100 |
| beta (β) | 1/5 | 1/10 | 1/10 | 1/10 |

*Nstep is the number of time steps for the crack to advance one half the element length.

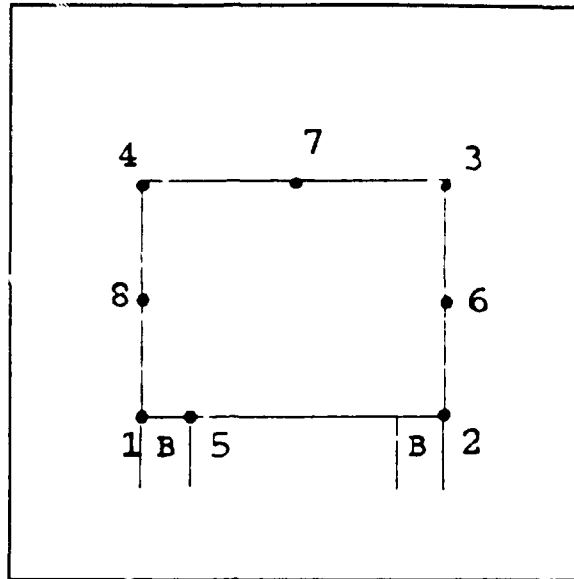


Figure 5. Relationship of beta to element length

D. STUDY ON MASS AND STIFFNESS MATRICES

As indicated in [Ref. 11], test cases have shown that the diagonal matrix, using the procedure outlined in Chapter II, gives greater accuracy than a consistent mass matrix. A diagonal mass matrix also requires less storage space than a consistent mass matrix and simplifies the computation of the central difference scheme.

For the regular eight noded isoparametric element, the concentrated mass at the corner nodes are one-eighth that of the mid-nodes. For the moving nodal case, the diagonalized mass matrix from the moving node element caused unstable (oscillatory) conditions. Because of the close proximity of

moving node five to node one, the diagonal mass matrix procedure resulted in the majority of the mass concentrated at nodes five and one. As node five moved across the edge of the element toward the center, the nodal point mass approached that of the regular element. Due to the unstable conditions resulting from the diagonal mass procedure for the moving node element, the diagonal mass matrix was calculated with the moving node at the center of the element boundary edge. The computed diagonal mass matrix remained constant throughout the analysis.

For the eight noded regular element the element nodal stiffness remained constant. On the other hand, for the eight noded moving node element the nodal stiffness of nodes one, two, and five varied as node five moved along the edge of the element. Node five carried the higher stiffness. The remaining nodes (three, four, six, seven, eight) were equivalent to the regular element.

E. COMPARISONS OF ENERGY TERMS

In order to make a direct comparison between the use of a stationary element and a transition element, the generated results were compared with Broberg's problem. The finite element breakdown for Broberg's problem was as depicted by Kobayashi et al. [Ref. 5] and as shown in Figure 8.

Figure 9 shows the crack opening displacement during crack propagation. The two finite element results are compared to

the analytical solution as solved by Broberg. Except for some positions, the results were relatively similar. No comparative conclusion can be drawn from the results. Although their close comparison to the analytical solution indicates the reasonableness of the model.

Figure 10 shows the crack opening displacement at $x = 0$. From this result, it is seen that the use of the moving node element approximates a propagating crack more closely than the stationary element.

Figure 11 shows the work on the plate during crack propagation. There is a similar trend between the stationary element and the moving node element with the exception that there is a slight increase in the work for the moving node element.

Figure 12 shows the calculated strain energy during crack growth. The stationary element produces spurious oscillation. The oscillation is caused by the instant release of the crack tip during the process of discrete crack tip advances [Ref 5]. As shown in Figure 12a, there was a rapid build up in the strain energy until the node was released. Upon nodal release there was a rapid reduction in the strain energy followed by a rapid increase until the next nodal release. The oscillation amplitude of the strain energy increased during crack propagation. Employing a moving node element made the crack tip movement more continuous. As a result, the oscillation amplitude of the strain energy was much reduced, Figure 12b.

Figure 13 shows the calculated kinetic energy during crack growth. The delayed nodal release, caused by the stationary element, resulted in a rapid decrease in the kinetic energy prior to the release of the node, then a rapid increase followed by a rapid reduction until the next nodal release. This trend was a reversal of that seen for strain energy. The oscillation amplitude of the kinetic energy increased during crack growth as it did for the strain energy. Employing a moving node element reduced the oscillation amplitude because the moving node better represents a moving crack tip.

Although not necessary since the crack had already passed, if variable interpolation was used to move the middle node (node five) back to the center position, there was an increase in the oscillation of the results. The increase in oscillation is probably due to the abrupt change in the nodal stiffness when bringing node five back to its center location. As the crack propagated, there was a gradual shift in the stiffness of node five.

In an elastic medium there are only two types of waves that propagate through a solid that is unbounded [Ref. 16]. These are dilatational and distortional waves. If the solid has a free surface, Rayleigh surface waves may also propagate. Rapid reduction in stress occurred upon nodal release. Due to this rapid reduction, unloading waves were generated at the crack tip. As the wave propagated through the medium, strain energy decreased and kinetic energy increased.

If the body is bounded, elastic waves reflect and refract off the boundaries back toward the crack tip as loading waves. The loading wave expands the body; thereby, amplifying the strain caused by the tension load. This result of an increase in strain energy is seen in Figure 13a.

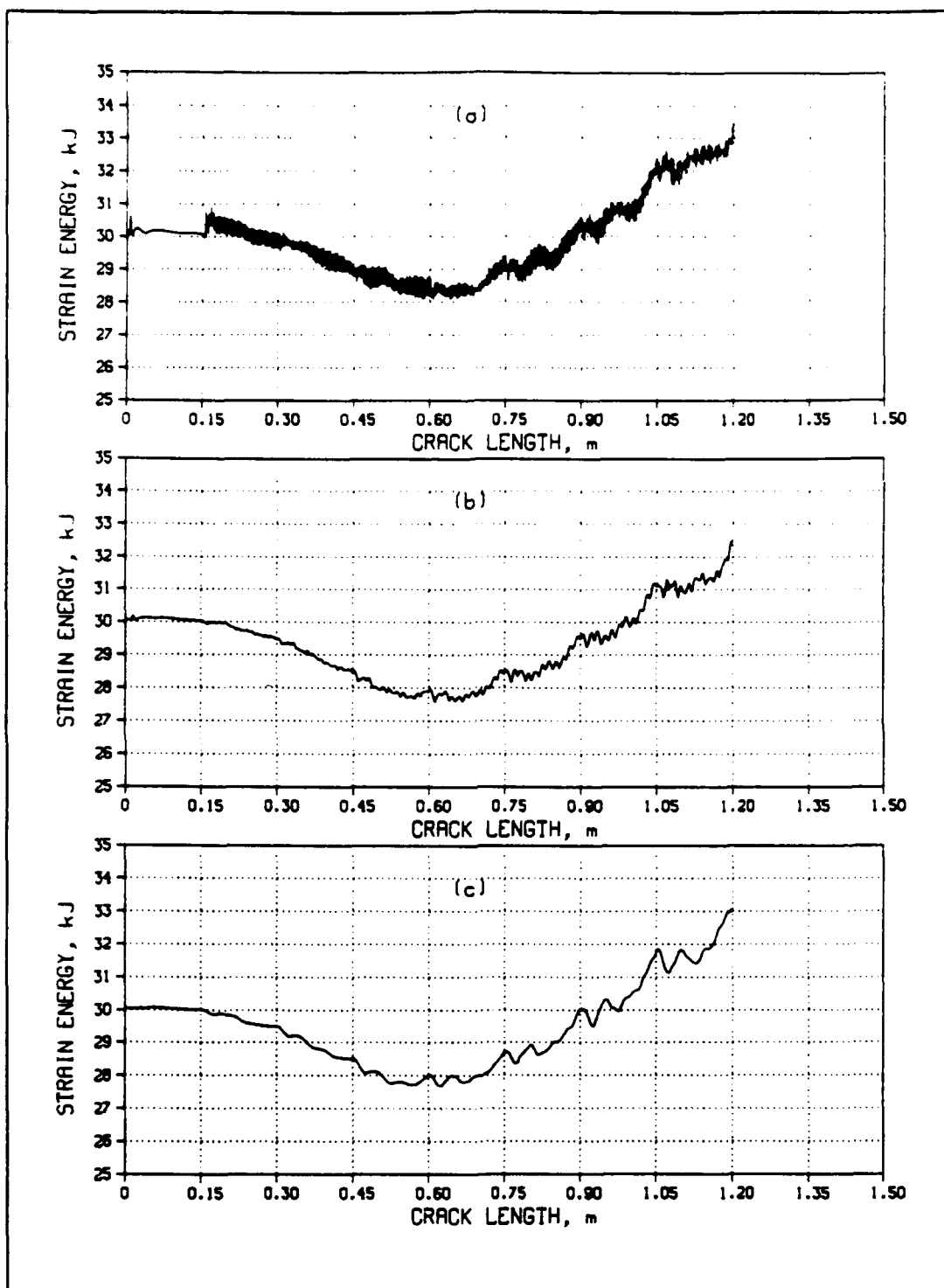


Figure 6. Effect of varying beta on strain energy for nstep1 = 50: (a) beta = 1/20, (b) beta = 1/10, (c) beta = 1/5.

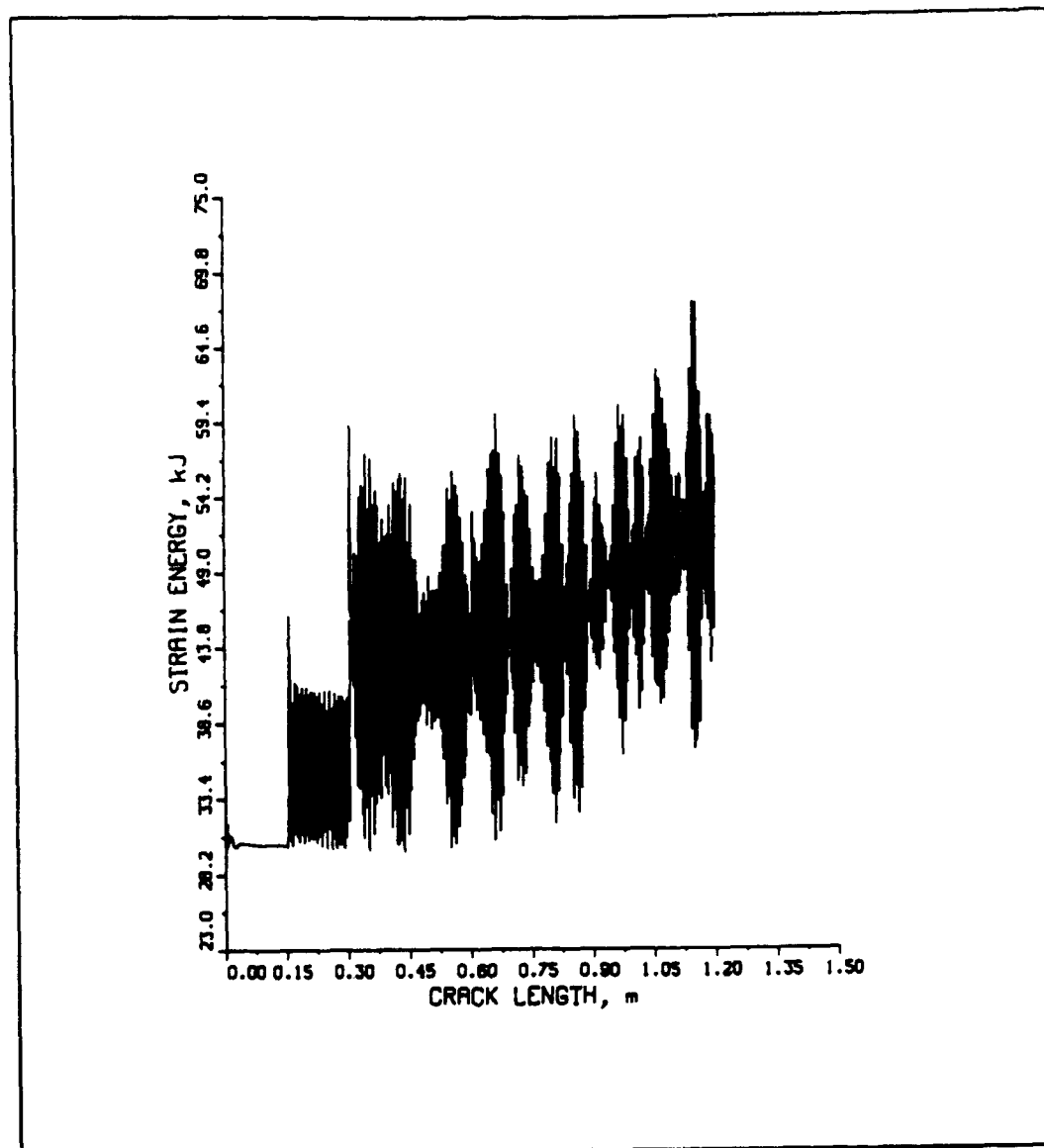


Figure 7. Effect when node five is too close to corner node

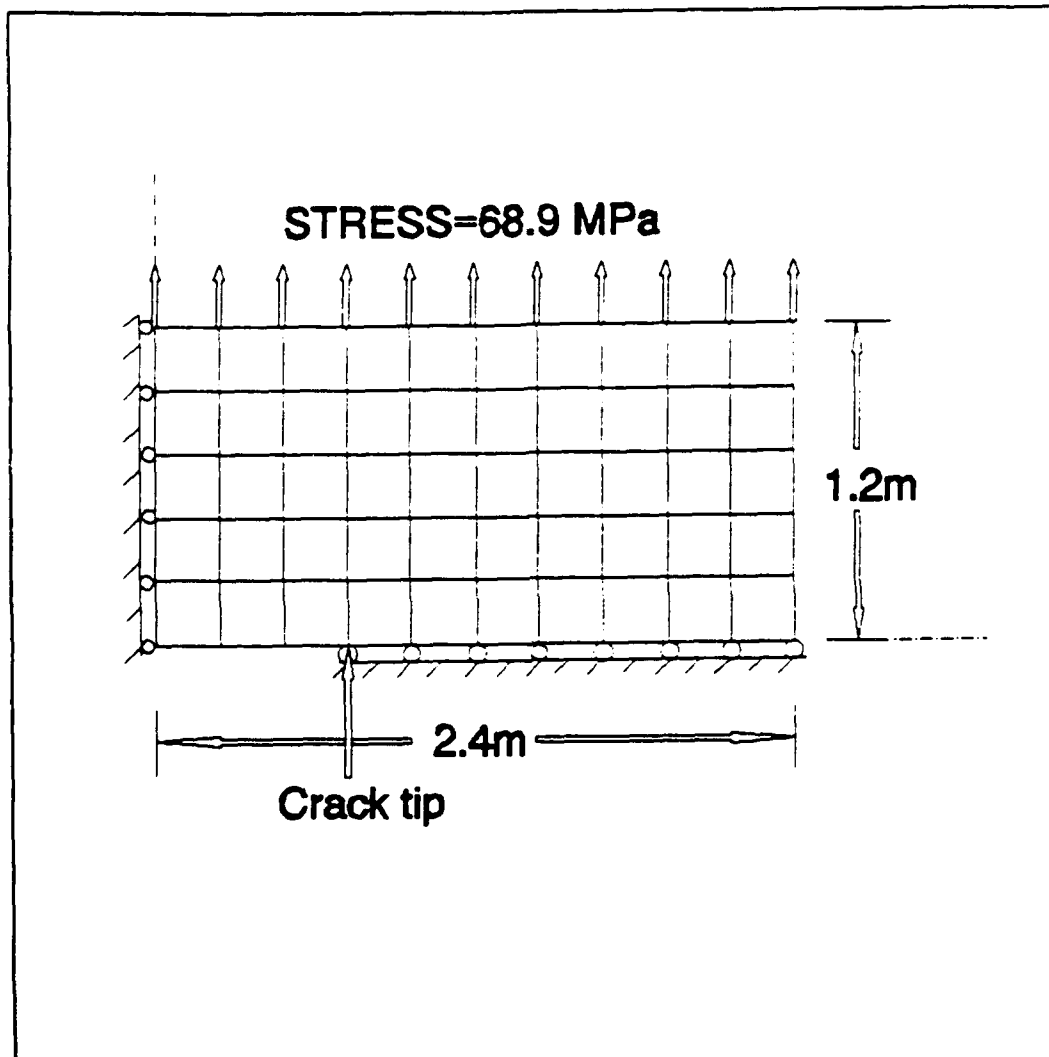


Figure 8. Finite element mesh for Broberg's problem

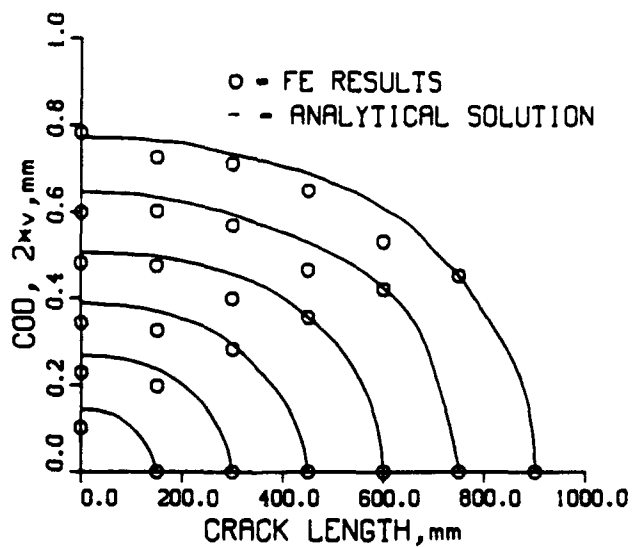
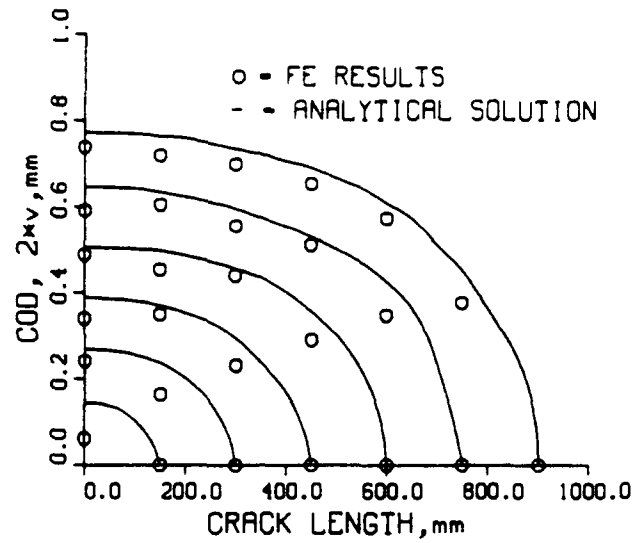


Figure 9. Crack Opening Displacement for (a) stationary element and (b) moving node element

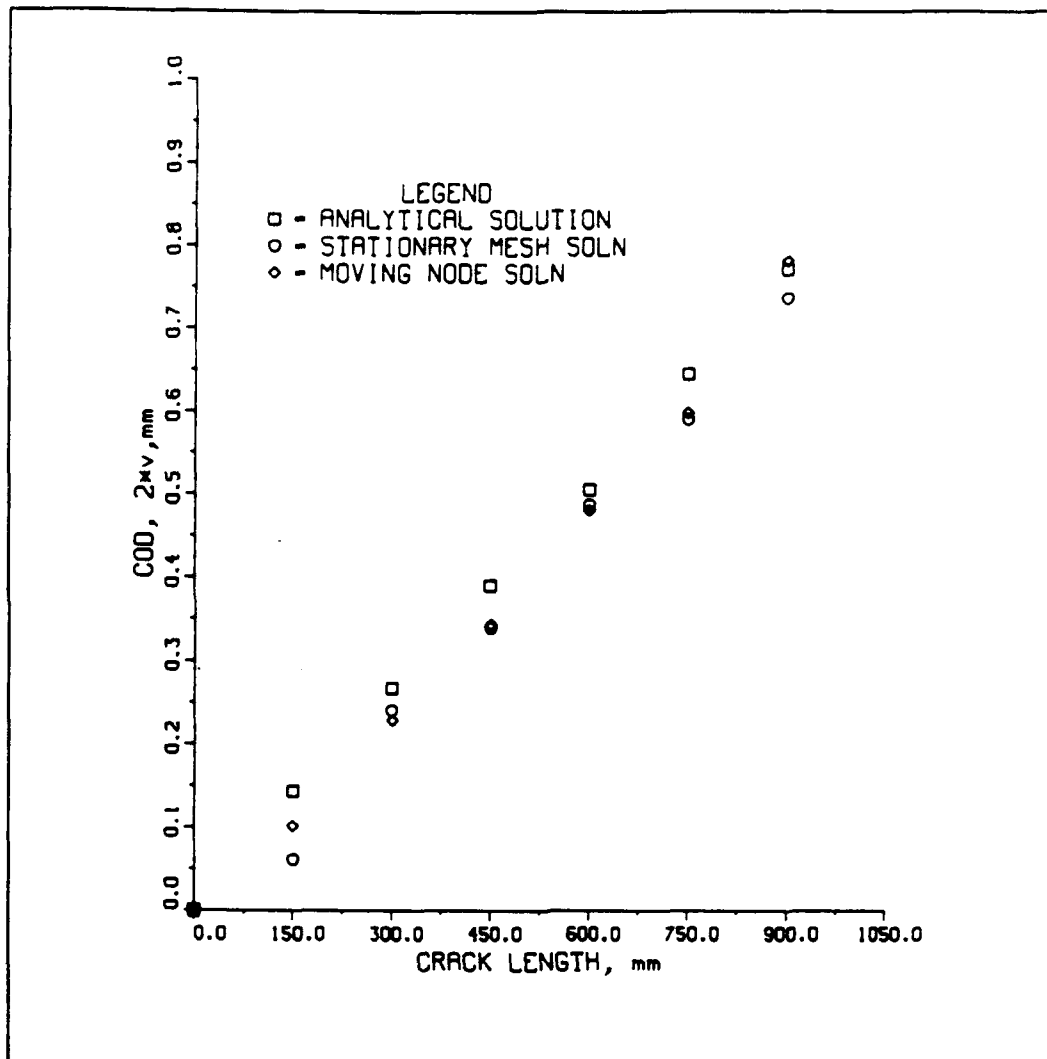


Figure 10. Crack opening displacement at $x = 0$

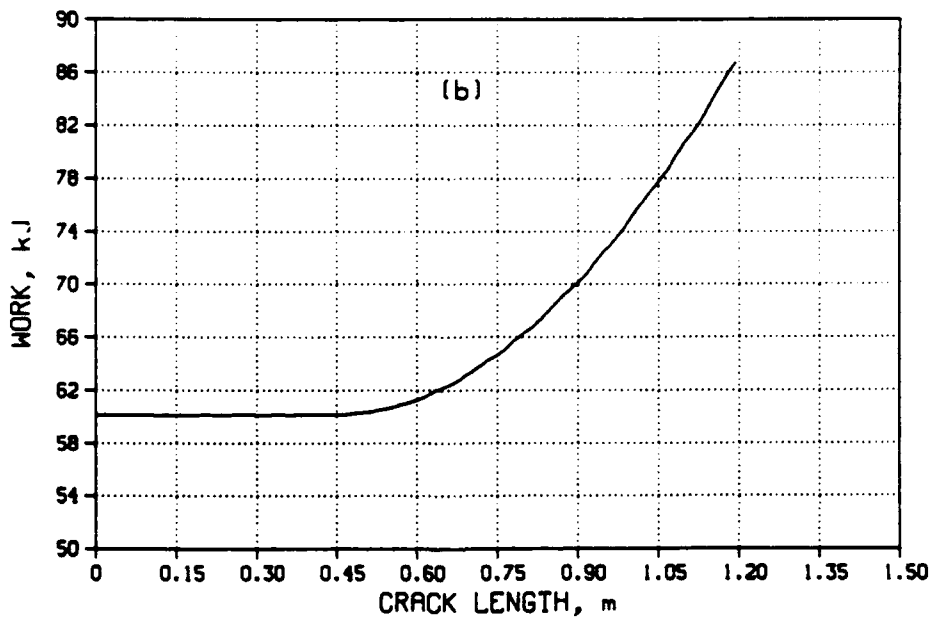
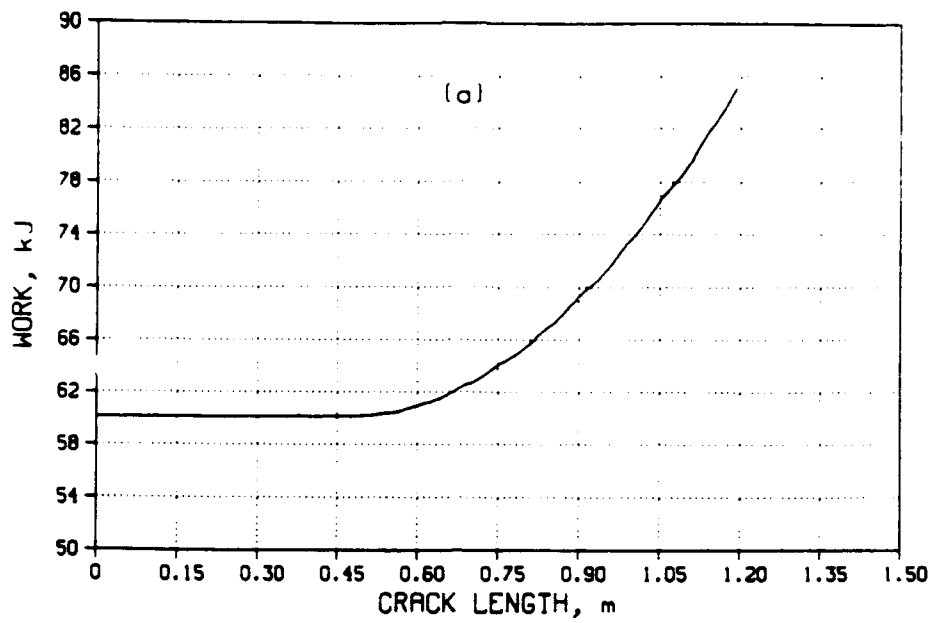


Figure 11. Work vs Crack Length (a) stationary element, (b) moving node element ($\beta=1/5$)

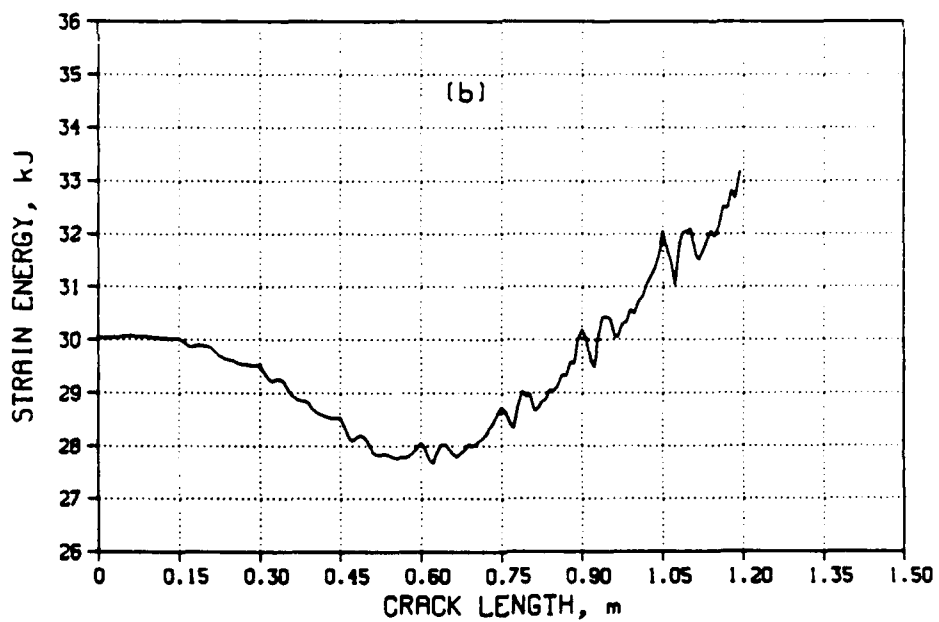
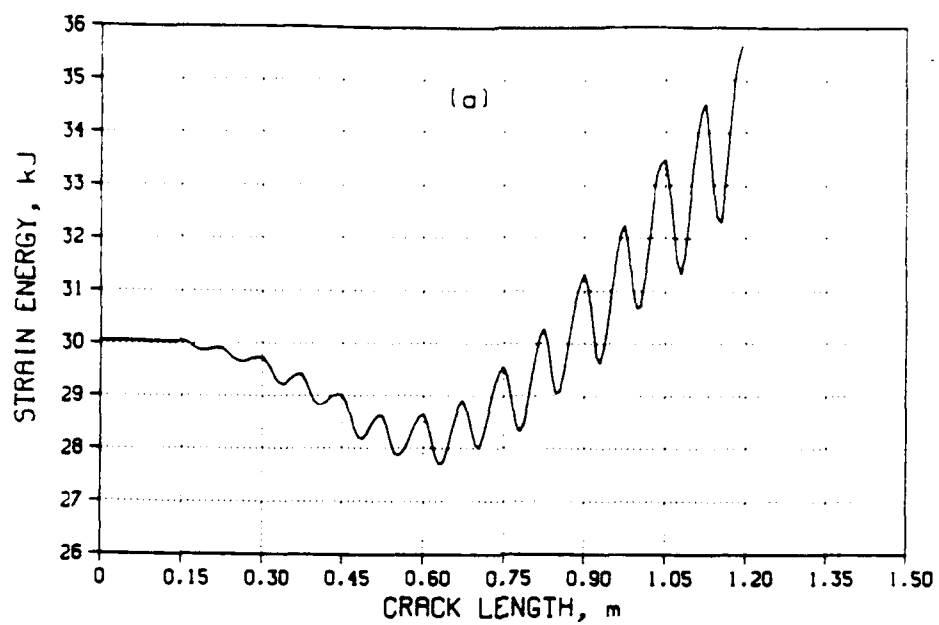


Figure 12. Strain energy vs Crack Length for (a) stationary element (b) moving node element ($\beta=1/5$)

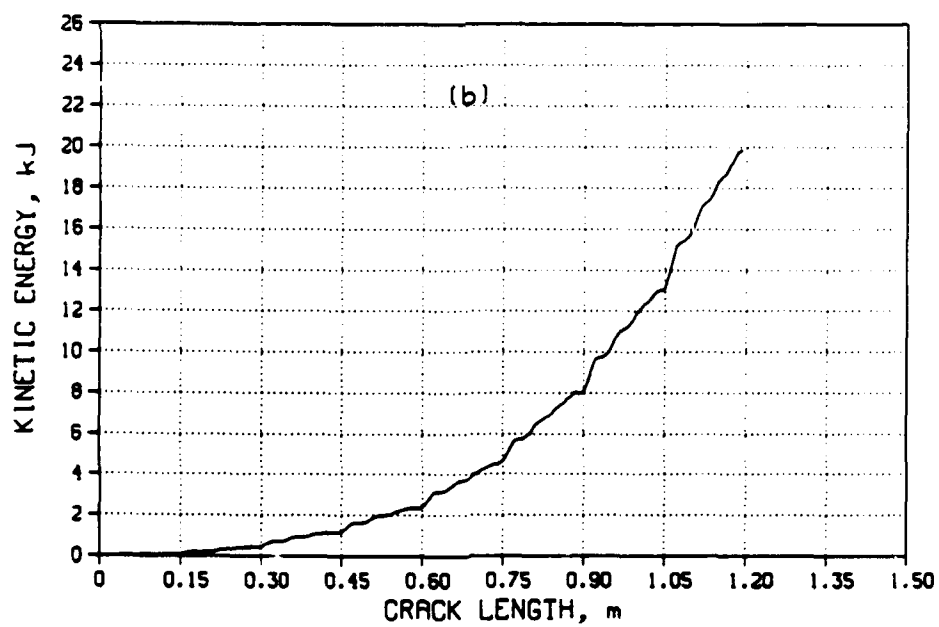
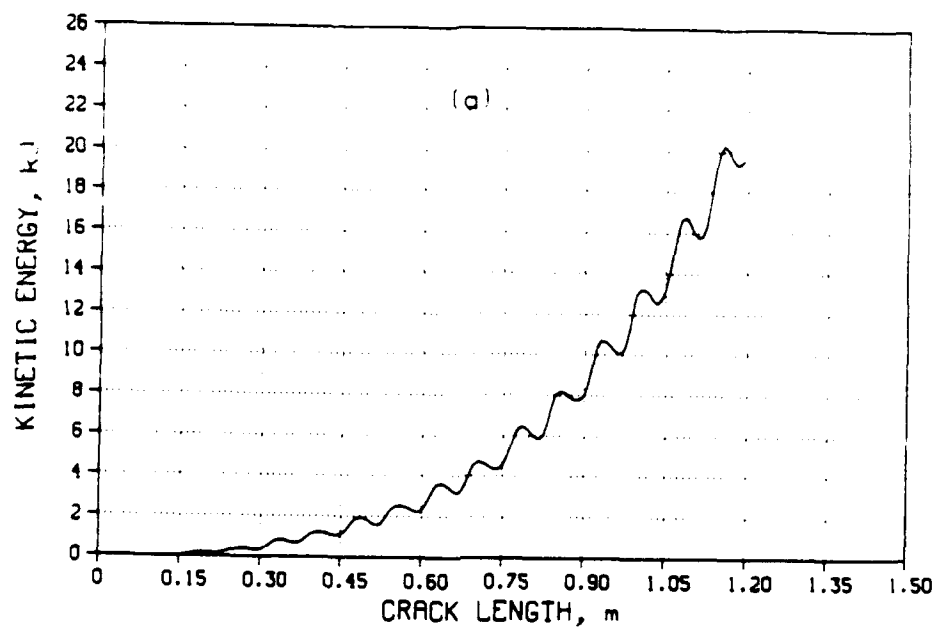


Figure 13. Kinetic energy vs Crack Length for (a) stationary element (b) moving node element ($\beta=1/5$)

IV. CONCLUSIONS AND RECOMMENDATIONS

This study focused on the finite element modeling of a rapidly propagating crack. Two methods were employed in this study. The first procedure, adopting stationary elements, resulted in spurious oscillation of the energy terms. For this procedure the propagating crack was represented by discrete jumps at given time intervals. To more closely approximate the propagating crack, a moving node procedure was employed in the model. As shown in the previous chapter, the moving node procedure reduced the spurious oscillation of the energy terms. Unlike the moving mesh procedure, no remeshing is required for this procedure.

From the comparison of the two procedures mentioned above, the following observations were noted:

1. The two forms of the central difference methods yield almost the same results. As a result, the "summed form" was preferred due to its simplicity and efficiency in computational time.
2. The range which the moving node, which represents the crack tip, can propagate along the edge of the element was a function of the time step size for relatively large time step sizes. However, for reduced time step sizes, the range was the same.

3. For the moving node procedure, diagonalizing the mass at each increment of movement resulted in sporadic results. When node five is close to the corner nodes the majority of the concentrated element mass was located at node five and the respective corner node it was close to.

This study did not account for the singularity in the crack tip. To represent the stress field near the crack tip more accurately, it is recommended that singular element, as derived in [Ref. 9], be incorporated into the model.

LIST OF REFERENCES

1. Kanninen, M.F., and Popelar, C.H., Advance Fracture Mechanics, Oxford University Press, 1985.
2. Kanninen, M.F., "A Critical Appraisal of Solutions in Dynamic Fracture Mechanics", Numerical Method in Fracture Mechanics", pp. 612-633, 1977.
3. Kobayashi, A.S., Emery, A.F., and Mall, S., "Dynamic-finite-element and Dynamic-photoelastic Analyses of Two Fracturing Homalite-100 Plates", Experimental Mechanics, Vol.16, No.9, pp.321-328, September 1976.
4. Malluck, J.F., and King, W.W., "Fast Fracture Simulated By A Finite-Element Analysis Which Accounts For Crack-Tip Energy Dissipation", Numerical Method in Fracture Mechanics, pp.648-659, 1978.
5. Kobayashi, A.S., Mall, S., Urabe, Y., and Emery, A.F., "A Numerical Dynamic Fracture Analysis of Three Wedge-Loaded DCB Specimens", Numerical Methods in Fracture Mechanics, pp.673-684, 1977.
6. Nishioka, T., and Atluri, S.N., "Computational methods in dynamic fracture", Computational Methods in Mechanics of Fracture, pp.335-383, 1986.
7. Nishioka, T., and Atluri, S.N., "Numerical Modeling of Dynamic Crack Propagation in Finite Bodies, by Moving Singular Elements-Part I: Formulation," ASME Journal of Applied Mechanics, Vol.47, pp.570-576, September 1980.
8. Banks-Wills, L., "Quarter-Point Singular Elements Revisited", International Journal of Applied Mechanics, Vol.34, pp.R63-R69, 1977.
9. Kwon, Y.W., and Akin, J.E., "Development of a Derivative Singular Element for Application to Crack Problems", Computers and Structures, Vol.31, No.3, pp.467-471, 1989.
10. Akin, J.E., Application and Implementation of Finite Element Methods, Academic Press, Inc., 1982.
11. Cook, R.D., Concepts and Applications of Finite Element Analysis, 2d ed., John Wiley & Sons, 1981.

12. Bathe, K.J., Finite Element Procedures In Engineering Analysis, pp.499-556, Prentice-Hall, Inc., 1982.
13. Park, K.C., "Practical Aspects Of Numerical Time Integration", Computers and Structures, Vol.7, pp.343-353, 1977.
14. Owen, D.R.J., and Shantaram, D., "Numerical study of dynamic crack growth by the finite element method", International Journal of Fracture, Vol.13, No.6, pp.821-837, December 1977.
15. Callister, W.D., Material Science and Engineering, 2d ed., pp.196-204, John Wiley & Sons, Inc., 1991.
16. Kolsky, H., Stress Waves in Solids, pp.4,84-86, Oxford University Press, 1953.
17. Broberg, K.B., "The propagation of a brittle crack", Arkiv for Fysik, Vol.18, pp.159-198, 1960.

INITIAL DISTRIBUTION LIST

| | No. Copies |
|---|------------|
| 1. Defense Technical Information Center Cameron Station Alexandria VA 22304-6145 | 2 |
| 2. Library, Code 052 Naval Postgraduate School Monterey CA 93943-5002 | 2 |
| 3. Professor Y.W. Kwon, Code ME/Kw Department of Mechanical Engineering Naval Postgraduate School Monterey, CA 93943-5000 | 2 |
| 4. Naval Engineering Curricular Office, Code 34 Naval Postgraduate School Monterey, CA 93943-5000 | 1 |
| 5. Clifford T. Christy 94 Diamond St New Haven, CT 06515 | 1 |
| 6. Dr. Rembert Jones, Code 172 Submarine Structures Division Naval Surface Warfare Center, Carderock Div. Bethesda, MD 20084-5000 | 1 |
| 7. Dr. Y. D. Rajapakse Office of Naval Research Mechanics Division, Code 1132 800 North Quincy Street Arlington, VA 22217-5000 | 1 |
| 8. Mr. David Bonnani Naval Surface Warfare Center, Carderock Div. Code 1720.2 Bethesda, MD 20084-5000 | 1 |
| 9. Dr. Phillip B. Abraham Office of Naval Research Mechanics Division, Code 1132 800 North Quincy Street Arlington, VA 22217-5000 | 1 |